Desalination by Electrodialysis Using a Stack of Patterned Ion-Selective Hydrogels on a Microfluidic Device

Burcu Gumuscu, A. Sander Haase, Anne M. Benneker, Mark A. Hempenius, Albert van den Berg, Rob G. H. Lammertink, and Jan C. T. Eijkel**

This study reports a novel approach for separation of charged species using anion-exchange hydrogel (AEH) and cation-exchange hydrogel (CEH) in a microfluidic device. The capillary line pinning technique, which is applied in this study, enables in situ fabrication of alternating AEH and CEH that are placed in confined compartments. Adjacent enriched and depleted streams are obtained in continuous flow when a potential difference is applied over the hydrogel stack. The desalination performance of the microchip is demonstrated at different salt concentrations (0.01×10^{-3}–1×10^{-3} M sodium chloride), potentials (10–100 V), current densities (12–28 A m^{-2}), and liquid flow rates (0–5 µL min^{-1}). It is shown that the microchip is able to remove ≈75% of the salt initially present in the depleted outlet streams at inlet stream concentrations of 1×10^{-3} M sodium chloride. Besides desalination, the microchip allows study of ion transport in the ion-selective hydrogels to elucidate the interplay of transport phenomena at the electrolyte–hydrogel interface during the desalination process.

1. Introduction

Membrane stacks are widely used for electrodialysis (ED) and reverse electrodialysis (RED) in macroscale systems.[1–3] Alternating cation (cation-exchange hydrogel (CEH)) and anion-selective membranes (anion-exchange hydrogel (AEH)) are stacked with spacers to allow a flowing electrolyte solution between the membranes. When an electric field is applied to this system, the anions in the electrolyte solution will migrate toward the anode, while the cations migrate toward the cathode. However, anions and cations will be blocked from moving through the CEM and AEM respectively, resulting in the formation of alternating depleted and enriched flow streams. As the applied electric field strength is increased, the ion transport rate and therefore the current in the system will rise—up to a critical point. Beyond this point, the system enters the well-known limiting current regime,[4] where the current no longer increases with electric field strength, and the energy efficiency of the ion separation process is reduced. In this regime, the major resistance for ion transport is located in the boundary depletion layer which is formed adjacent to the membrane. When increasing the electric field strength further or in the case of membrane discharge (resulting in lower charge density) due to the developing pH profile in the membrane, the over-limiting current regime can be reached. In this over-limiting current regime, additional ions are transported, generated through either water splitting or hydrodynamic effects.[5,6] Water splitting can also lead to a developing pH profile in the membrane that can give rise to a change in membrane charge density. The hydrodynamic and ion transport phenomena can result in a loss of performance for macroscale ED systems.[7–9]

Microfluidic desalination systems have been applied for two purposes. First, microfluidics has been used for downscaling the ED process to provide more insight into the ion transport phenomena that occur at the microscale.[10] Thanks to the advances in microfabrication techniques, ion-selective materials have been integrated in fluidic platforms, increasing the experimental investigations of the aforementioned phenomena.[11] Kim et al. fabricated two microchannels separated by a Nafion membrane, which was fabricated using microstamping, to observe multiple vortical flows inside the ion concentration polarization (ICP) layer.[12] Kwak et al. fabricated a polydimethylsiloxane (PDMS) microchip consisting of externally mounted commercial ion exchange membranes for visualization of concentration and liquid flow profiles at ohmic, limiting, and overlimiting regimes.[13] Second, microfluidics has been used to manufacture miniaturized devices for desalination. Recently, in situ fabrication of hybrid membranes by photolithography has been demonstrated for charge-based separations in a glass microchip.[14] In another work, solvent

B. Gumuscu, Prof. A. van den Berg, Prof. J. C. T. Eijkel
BIOS Lab-on-a-Chip Group
MESA+ Institute for Nanotechnology
MIRA Institute for Biomedical Technology and Technical Medicine
University of Twente
Enschede 7500AE, The Netherlands
E-mail: b.gumuscu@utwente.nl; j.c.t.eijkel@utwente.nl

A. S. Haase, A. M. Benneker, Prof. R. G. H. Lammertink
Soft Matter, Fluidics, and Interfaces
MESA+ Institute for Nanotechnology
University of Twente
Enschede 7500AE, The Netherlands

Dr. M. A. Hempenius
Materials Science and Technology of Polymers
MESA+ Institute for Nanotechnology
University of Twente
Enschede 7500AE, The Netherlands

DOI: 10.1002/adfm.201603242

evaporation was used for in situ fabrication of ion-selective membranes in a PDMS microchip consisting of dual channels for studying ICP phenomena in both desalination (up to 99%)[15] and pre-concentration[16] modes.

The aforementioned methods for incorporation of membranes into microfluidic systems pose challenges in terms of robustness, consistency, and ease of fabrication. For example, photolithography techniques bring alignment problems, while evaporation bears the risk of damaging the membranes. Integration of pre-fabricated membranes in microfluidic chips can furthermore lead to liquid leakage.[17] In situ fabrication of membranes in microchips is an alternative, but is cumbersome when using, for instance, interfacial polymerization.[18] Hydrogels provide an alternative to membranes, and have been successfully incorporated in microfluidic devices in the past.[14,19] Previously, we introduced the capillary line pinning technique for controllable patterning of hydrogels in microchips.[20] Due to their facile integration, hydrogels are promising candidates to manufacture desalination devices as well as study the hydrodynamic and ion transport phenomena in microfluidic devices, as they provide an ion-selective and hydrophilic matrix, which is versatile, inexpensive, and tailorable.[14,18]

In this work, we present a microfluidic device consisting of a stack of alternatingly-patterned, oppositely-charged hydrogel patches fabricated by capillary line pinning for performing ED. To the best of our knowledge, the use of such a platform has not been demonstrated or investigated before for microfluidic ED. As a proof of principle, the periodic hydrogel patches were used to obtain alternatingly diluted and enriched parallel streams under different flow rates and applied potential differences. In this proof of concept, low-concentration salt solutions were desalinated due to the low charge density in the hydrogels. This platform also allowed us to study ion transport through the hydrogels, and salt concentration fluctuations and ICP in the microchannels, for which purpose we used a negatively charged fluorescent dye, Alexa Fluor 488 Cadaverine. The ability to visualize charge transport in the hydrogels helps to obtain a better understanding of hydrodynamic and ion transport phenomena that occur in ED and RED systems. Besides that, PDMS microchips with in situ patterned hydrogels enable low-cost and versatile platforms for microfluidic ion-separations such as desalination.

2. Results and Discussion

2.1. Characterization of Hydrogels

Figure 1a shows an assembled microchip with PDMS pillars and capillary barriers. In the microchip design, each hydrogel compartment (200 × 500 µm), is connected to another via microchannels. **Figure 2** outlines the microchip fabrication and hydrogel patterning processes. In Supporting information S1, the molecular structures of charged monomers ([2-(methacryloyloxy)ethyl]trimethylammonium chloride (METC) and 3-sulfopropyl acrylate potassium salt (SPAP)) photopolymerized with acrylamide and bis (*N*,*N*′-bis(2-hydroxyethyl)ethylenediamine) are shown. The free radicals yielded by 2,2-dimethoxy-2-phenylacetophenone (DMPA) started the crosslinking process by randomly associating with acrylamide, bis, and METC or SPAP monomers and grew polymer chains, which eventually became polymerized in the illuminated region. The photopolymerization process has been explained in detail in our previous work.[21] The scanning electron microscopy (SEM) images indicate that the hydrogels obtained after photopolymerization were homogeneous (Supporting information S2).

METC and SPAP are suitable monomers to obtain charge selective interfaces for ED because they have permanent positive and negative charge densities, respectively, which is pH independent in the range of pH 2–12.[22,23] In addition, the hydrolytic stability of METC and SPAP polymers enables charge-based separations in ED microchips.[22,23] In the previous studies, both charged monomers have shown to be superabsorbents, which results in a strong swelling behavior.[24,25] The swelling behavior was suppressed by increasing the crosslinking density and the amount of uncharged monomers in this work. We measured the water swelling of the bulk METC and SPAP polymers as 460% ± 10% for METC and as 450% ± 10% for SPAP after drying the bulk materials in a vacuum oven (**Table 1**). The high swelling degree indicates the ability of the hydrogels to absorb water in high contents,

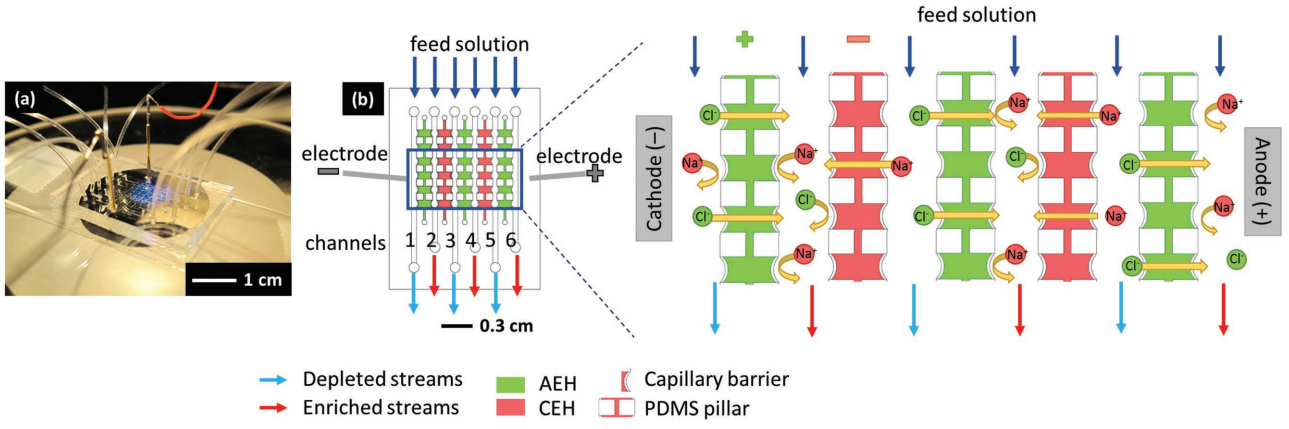

Figure 1. a) Image of the assembled microchip. b) Schematic representation of a membrane stack containing alternating AEHs and CEHs and the desalination mechanism.

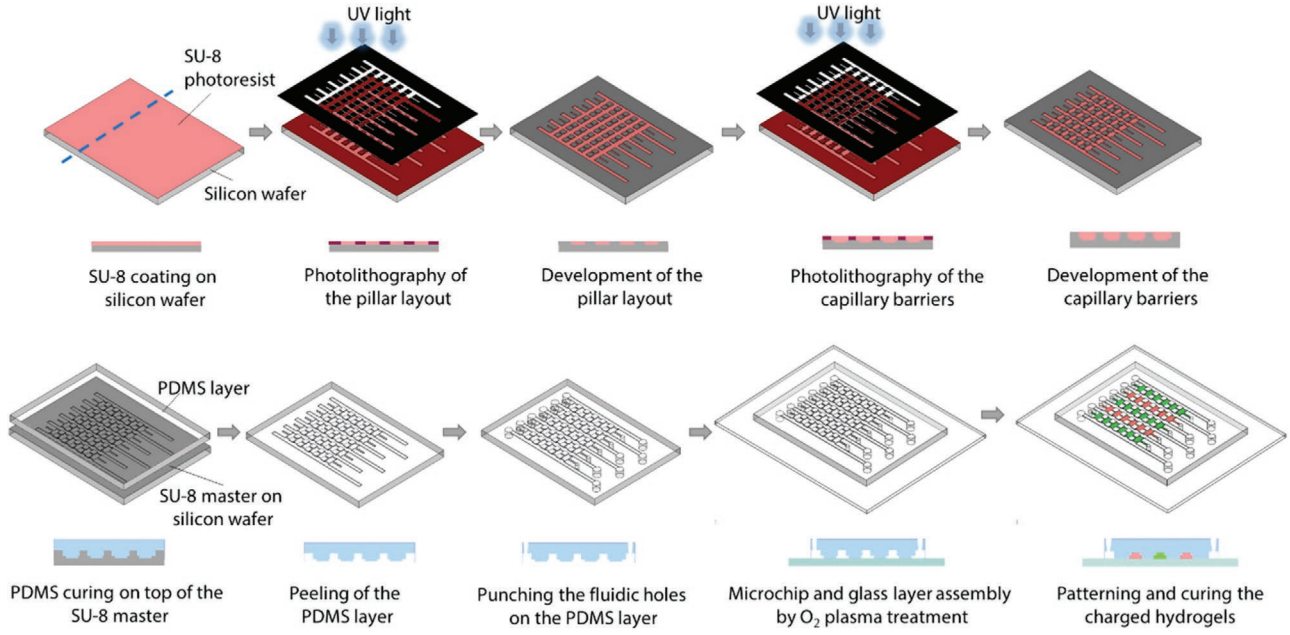

Figure 2. Photolithography and soft lithography procedures. The schematics on the top line illustrate the photolithography and the schematics on the bottom line present the soft lithography process flows. Dashed line represents the cross-sectional area.

which is related to the hydrophilic nature of the PA backbone. Note that directly after photopolymerization, the hydrogels already have a high water content right, so that when immersed in deionized water, the additional swelling of the bulk hydrogels was measured to be only 15% and 16% for AEH and CEH, respectively. Both hydrogels showed an identical swelling behavior also in the microchip as shown in Supporting information S3. In addition, hydrogels immersed in salt solutions are expected to swell less than in deionized water.[26] The reason is that hydrogel swelling decreases with increasing ion concentration, as the charged side groups present in the hydrogels are increasingly screened by the ions in the salt solution.[27,28]

The presence of cross-linker and SPAP or METC was verified using Fourier transform infrared spectroscopy (FTIR). The FTIR spectra shown in **Figure 3** verified the presence of SPAP sulfonate groups from S=O stretching bands at 982 and 1043 cm^{-1} and a SO_2 symmetric stretching absorption at 1178 cm^{-1}.[29] A relatively weak absorption at 1170 cm^{-1} was ascribed to N−CH_3 stretching of METC repeat units.[29] C−N stretching absorptions in general are known to be weak.[29,30] We measured the FTIR spectra of the corresponding monomers to confirm the location of the peaks observed in the polymers (Supporting information S4).

We also analyzed the chemical composition of the hydrogels using X-ray photoelectron spectroscopy (XPS) to verify the presence of either SPAP or METC monomers. The atomic ratios of carbon, nitrogen, oxygen, sulfur, chlorine, and potassium are shown in **Table 2**. METC and SPAP polymers were compared with PA polymer for the evaluation of the atomic percentage changes. In METC polymer, the amount of carbon atoms remained the same despite the expectation of a slight increase.[30] The nitrogen atom content remained the same, which was consistent with the expected composition. The amount of oxygen was expected to increase, which was consistent with the measurements in Table 2. The detection of chloride clearly showed the presence of charged N^+ groups.[31,32] In the SPAP hydrogel, the content of carbon atoms decreased, which could be an experimental artefact. On the other hand, the amount of nitrogen atoms remained the same, as expected by considering the molecular formulas. The amount of oxygen atoms increased significantly and this can be attributed to the high oxygen content of the SPAP monomer.[30] Next, the presence of sulfonate groups was validated by the detection of sulfur atoms and potassium atoms. The latter, however, was present in a lower amount than expected. Here, the potassium atoms might be out of the scanning range due to the orientation of the charged groups on the polymer film.

Table 1 shows the material characteristics of the anion exchange (METC) and cation exchange (SPAP) hydrogels. Compared to commercially available ion exchange membranes,[33,34] METC exhibited a comparable and SPAP a low ion exchange

Table 1. Bulk material characteristics of cross-linked METC and SPAP polymers, with the 95% confidence interval of the mean indicated. All measurements have been repeated three times.

	AEH (METC)	CEH (SPAP)
Swelling in deionized water (%)	460 ± 10	450 ± 10
Ion exchange capacity (mmol g_{dry}^{-1})	1.95 ± 0.45	0.64 ± 0.09
Charge density (mol L_{H2O}^{-1})	0.43 ± 0.10	0.14 ± 0.02
Resistivity (Ω cm) (single meas.)	310	470
Permselectivity (%) (single meas.)	29	26

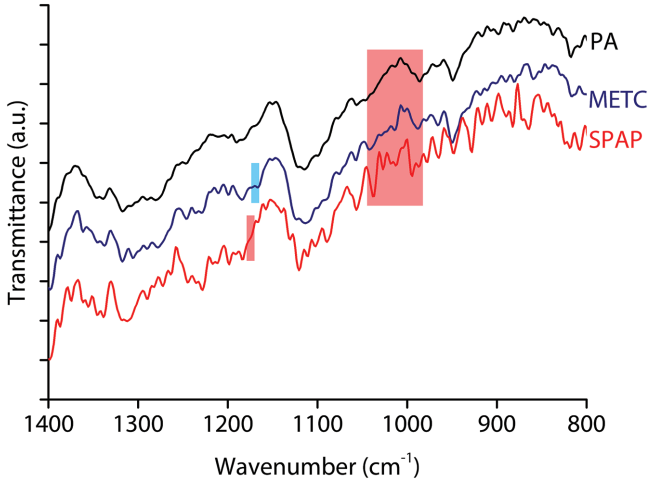

Figure 3. FTIR spectra of binary component ionic hydrogels. The compositions of METC + polyacrylamide (blue column), SPAP + polyacrylamide (red column), and only polyacrylamide are shown.

capacity. When considering the charge density, we found that both hydrogels, in comparison to commercially available membranes (for example, Neosepta AMX has a charge density of 4.8 M and Neosepta CMX has a charge density 5.7 M),[35] have a low number of charged groups per gram of water. We attribute this to the hydrophilic structure of the hydrogels and their capability to hold large amounts of water in their polymeric meshes. This can explain the moderate permselectivity of both hydrogels, as the permselectivity of an ion-selective membrane is related to its charge density.[33,34,36] Both anion and cation exchange hydrogels are therefore not fully selective for the counter-ions, which has an adverse effect on the desalination efficiency. Low salt concentrations, however, will lead to a decreased screening of the charged groups in the hydrogels, promoting charge separation. To demonstrate the successful functioning of the platform, we therefore performed the desalination experiments using a maximal salt concentration of 1×10^{-3} M NaCl. This concentration is two orders of magnitude smaller than the salt concentration of 0.1 M/0.5 M, which is commonly used in permselectivity measurements. The resistivity of the hydrogels (measured in 0.1 M NaCl) is larger than that of a typical commercial membrane with an area resistance of 3 Ω cm^2 and a membrane thickness of 150 µm, giving a resistivity of 200 Ω cm.[34,35] The relatively high resistivity of our hydrogels is probably related to their low charge density, giving rise to a low concentration of mobile counterions.

Table 2. XPS results for the polymers with different compositions.

Element (%)	C (1s) 283 eV	N (1s) 399 eV	O (1s) 529 eV	S (2p) 164 eV	Cl (2p) 200 eV	K (2p) 293 eV
PA	64.6	16.3	18.7	–	–	–
SPAP + PA	62.1	16.1	20.3	1.2	–	0.1
METC + PA	64.4	16.3	20.1	–	0.5	–

2.2. Desalination—Proof of Principle Experiments

Upon filling the microfluidic channels with electrolyte solution and applying a gradually increasing potential (ΔU = 0–3 V), we observed migration of the fluorescent dye (and thus presumably of the ions) into the hydrogels. 5×10^{-6} M of Alexa Fluor 488 Cadaverine was utilized as a negatively charged fluorescent dye, which is considered pH insensitive and has a low degree of photobleaching.[37] As expected, AEHs were observed to have a high fluorescence intensity, as they absorb the negatively charged fluorescent dye as a counter-ion to a much greater extent than CEHs, where the dye is the co-ion.

To test whether the stack of charged hydrogels can be used for desalination purposes, we filled all microchannels with a diluted salt solution (0.1×10^{-3} M NaCl) and did not impose any flow through the microchannels. Upon application of a potential difference, depletion zones of the fluorescent dye formed adjacent to the hydrogels in the expected microchannels (which are channels 2 and 5 as shown in Figure 1b), while the average fluorescence intensity in the enriched microchannels increased. Snapshots of this observation are shown in Supporting Information S5a-c. These observations indicate that the hydrogels are charge-selective and thus can be used for desalination.

IV-sweeps were measured to determine the characteristic underlimiting, limiting, and overlimiting current regimes, which are well known for ion-selective membrane systems.[3,8,10] These measurements were performed for different NaCl concentrations (0.01×10^{-3}, 0.1×10^{-3}, and 1×10^{-3} M) and flow rates (2, 3, 5, and 10 µL min^{-1}). Relatively low salt concentrations and flow rates were used to avoid the possible adverse effects of high current densities (e.g., extensive electrode reactions, gas formation). The applied voltage was ramped up with steps of 1 V, with a speed of 10 s per voltage step. **Figure 4** shows the *IV*-curves for different salt concentrations. We observed higher currents for higher salt concentrations, indicating that the current in the ohmic regime is proportional to the ion concentration in the liquid. The maximum current, which is reached at the highest potential difference of ΔU = 50 V in the over-limiting current regime, does not scale one-to-one with the salt concentration.

Normalization of the current I by the maximum current I_{max} of the corresponding experiment indicates that for all concentrations the transport behavior is similar. At a potential difference of approximately ΔU = 6 V, ion transport transitions from the ohmic to the limiting current regime. At a potential difference of roughly ΔU = 22 V, the overlimiting current regime starts. Calculation of the derivative $dI/d\Delta U$ shows that at these points the slope of the $I(\Delta U)$-curve changes, indicating a change in the transport characteristics. The transition points are particularly apparent from the curves for 0.1×10^{-3} and 1×10^{-3} M NaCl. The fluctuations in current decreased with increasing salt concentration. Different flow rates did not lead to significant differences in measured currents. This can possibly be attributed to incomplete depletion of ions in the diluted streams, implying that there are still ions available for charge transport through the hydrogels for all flow rates.

At elevated voltages (ΔU > 10 V) we observed the development of ion depletion zones in the depleted microchannels. On the other hand, a local increase of fluorescence intensity

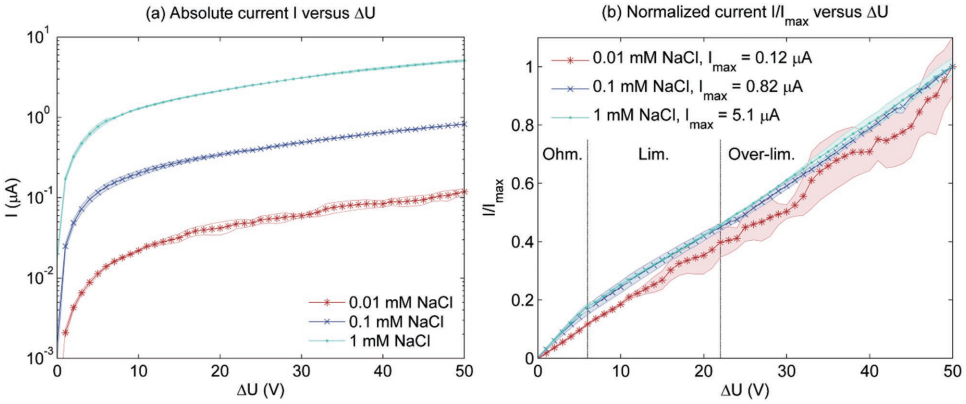

Figure 4. *IV* characteristics for different salt concentrations at flow rates of 3 μL min^{-1}. In panel (a), the absolute current *I* is plotted as function of the potential difference ΔU. The currents measured strongly depend on the salt concentration and scales accordingly. In panel (b), the currents are normalized by the maximum currect of the corresponding experiment. The graphs, in particular those for 0.1×10^{-3} and 1×10^{-3} M, show that around a potential difference of $\approx\Delta U = 6$ V and $\Delta U = 22$ V, the slope changes. This indicates the boundaries between the ohmic, limiting, and overlimiting current regimes.

was observed in the enriched microchannels, indicating the local existence of a higher salt concentration. As shown in **Figure 5**a, the depletion zones were observed to grow in size with increasing applied voltage and distance from the inlet. Figure 5b shows that for $\Delta U > 25$ V vortices were formed in the depletion zones. Probably because of the discontinuous nature of the hydrogel patches—an alternating pattern of charge-selective hydrogels and PDMS—the vortices did not migrate in the direction of the imposed flow as reported by Kwak et al.[13] At the upstream edge of each hydrogel patch, in the depletion zone, a high fluorescence intensity was observed. This suggests that near those points locally the salt concentration was larger than in the rest of the depletion zones. The mixing of the electrolyte solution next to the PMDS pillars by the vortices could explain this behavior, as this mixing increases the ion concentration near the PDMS pillar and consequently also near the upstream edge of each hydrogel. Charge transport is thus affected by the heterogeneity of the ion concentration at the hydrogel interface and could even enhance it when compared to a homogeneous ion-selective membrane, as previously discussed in the literature.[38]

For quantification of the desalination performance of the microchip, we performed measurements in which we applied a constant potential in the range of 0–100 V or a constant current in the range of 3–7 μA (current density of 12–28 A m^{-2}, where the area is defined as the hydrogel surface area per channel wall; for calculation of the area see Supporting Information S7). The resulting currents and potentials were measured to

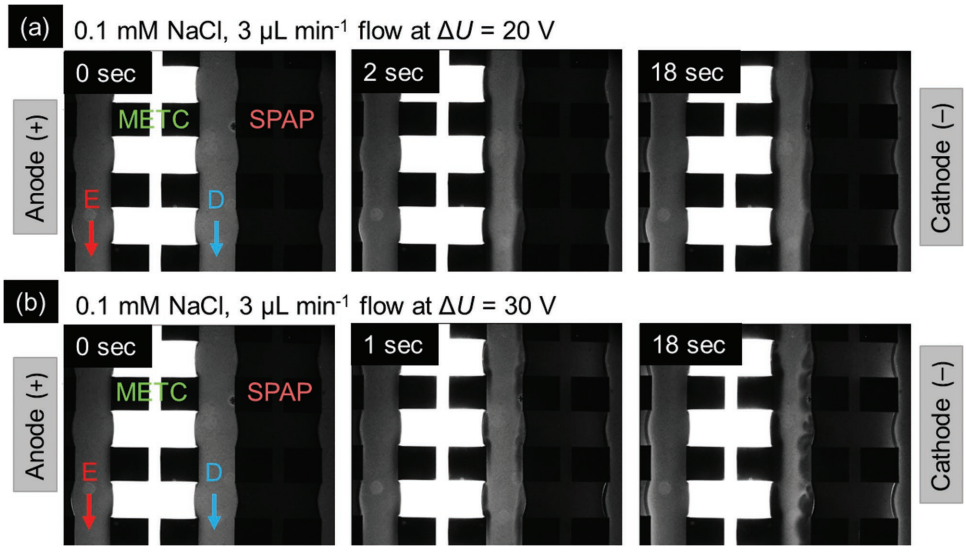

Figure 5. Fluorescence images showing the formation of ion depleted and enriched zones in the depleted (D) and enriched (E) microchannels for two constant potential measurements. 0.1×10^{-3} M NaCl solution with 5×10^{-6} M Alexa Fluor 488 Cadaverine (the fluorescent dye) was flushed through the microchip at 3 μL min^{-1}. The experiments were performed at a constant potential difference of a) $\Delta U = 20$ V and b) $\Delta U = 30$ V. The light-colored hydrogel is the anion-exchange hydrogel (METC) and the dark-colored one is the cation-exchange hydrogel (SPAP).

confirm charge transport through the hydrogel patches. A 1×10^{-3} M NaCl (supplemented with 5×10^{-6} M Alexa Fluor 488 Cadaverine) solution was pumped to the microchannels at either 3 or 5 µL min^{-1} flow rates. The conductivity of the solutions collected from the outlets was measured, and the salt concentration was calculated accordingly. As expected, the effluent streams from the microchannels were salt enriched or depleted in an alternating pattern.

In **Figure 6**a, the measured salt concentrations are shown for constant potential experiments for two different flow rates (3 and 5 µL min^{-1}). When the flow rate was increased, the residence time and therefore the charge separation decreased. Only the outlet streams of microchannels 2–5 were thereby taken into account. In the outer two microchannels 1 and 6, containing the electrodes and both facing only an anion-exchange hydrogel (see Figure 1), the solution is not expected to be either enriched or depleted because of the ions generated by the electrode reactions.

In **Figure 7**a, the current I is plotted as function of time t for a fixed potential difference of $\Delta U = 70$ V and a flow rate of 3 µL min^{-1}. This data corresponds to the results shown for 3 µL min^{-1} in Figure 6a. Figure 7a demonstrates that the average current during this experiment was 7.7 µA (31.3 A m^{-2}) at steady state. Based on this current, the total transport was calculated to be 4.8×10^{13} ions s^{-1}, while 6.0×10^{13} ions entered each channel per second. Based on this calculation, we expect a desalination degree of 80%. This is twice as high as the measured value of 40% for 3 µL min^{-1}, as Figure 6a shows. This deviation between the measured and expected desalination degree could be attributed to the low permselectivity of the hydrogels, which leads to nonselective ion transport in addition to the selective ion transport.

In Figure 6b, the salt concentrations of the outlet streams are shown for three applied currents, namely 3, 5, and 7 µA (12.2, 20.3, and 28.4 A m^{-2}). The data show that the outlet concentrations did not change when increasing the current I. Because the transport rate of charge carriers is proportional to the current, we would expect to see a difference in the degree of desalination. For all three currents, however, 75% of the initially present salt was removed in the desalinated streams. This suggests that this is the maximum degree of desalination that is achievable with these devices. As discussed in the previous paragraph, this can be attributed to the presently low charge density of the hydrogels. At higher currents then a lower efficiency is expected.

A valuable property of our microfluidic ED platform is that it enables real-time visualization of ion transport through the hydrogels using a fluorescent dye. This helps in obtaining a better understanding of the relevant electrokinetic transport phenomena. As the curve in Figure 7a shows, ≈600 s was required before the system reached steady state. We observe that at the very first instance ($t < 10$ s), the current decreased. This could indicate the buildup of a concentration boundary layer. Subsequently the current was increasing, reaching a (local) maximum at 250 s. Inspection of the fluorescence images for this experiment, given in Figure 7b, shows that the fluorescence distribution can be related to charge transport through the hydrogels. In the very first instance when applying a potential difference, a high concentration of negatively charged fluorescent dye was observed near the interface of the anion exchange METC-hydrogel with the salt-depleted channel. This fluorescent cluster of dye migrated toward the enriched channel in ≈250 s. Comparison with the current profile in Figure 6a shows that at that moment, the current reached a (local) maximum. Subsequently, the fluorescence slowly approached a constant intensity distribution, reaching steady state after ≈600 s. Note that not only in the positively charged AEH the fluorescence intensity and thus dye concentration increased, but also in the negatively charged cation-exchange SPAP-hydrogel (CEH). This indicates that, in line with the measured permselectivity of the bulk polymers, the ion selectively of the hydrogels was not perfect. The dye concentration, however, remained clearly larger in the AEH than in the CEH.

3. Conclusion

Alternatingly patterned AEH and CEH were fabricated in a PDMS microchip using capillary barriers. The chemical composition of the hydrogels was tailored to obtain a suitable

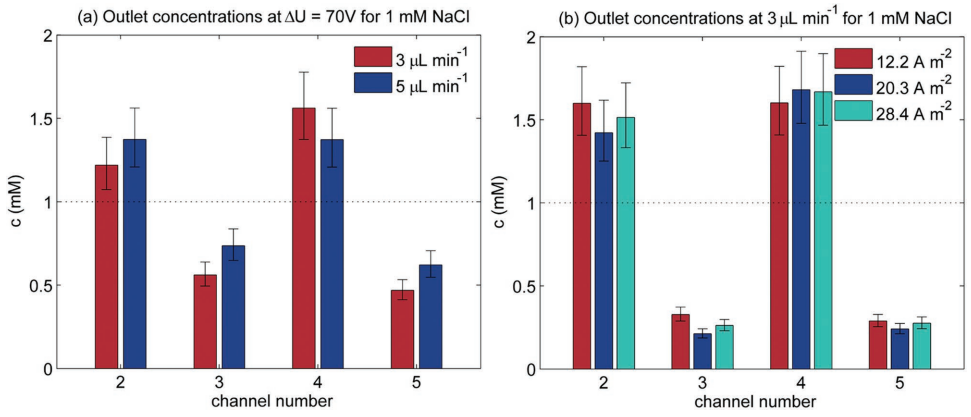

Figure 6. NaCl concentrations of the solutions collected from the outlets for a) constant potential measurements for different flow rates (3 and 5 µL min^{-1}) at a fixed potential difference of $\Delta U = 70$ V, and for b) constant current measurements for different current densities (12.2, 20.3, and 28.4 A m^{-2}) for a fixed flow rate of 3 µL min^{-1}. The error bars indicate the 95% prediction bounds.

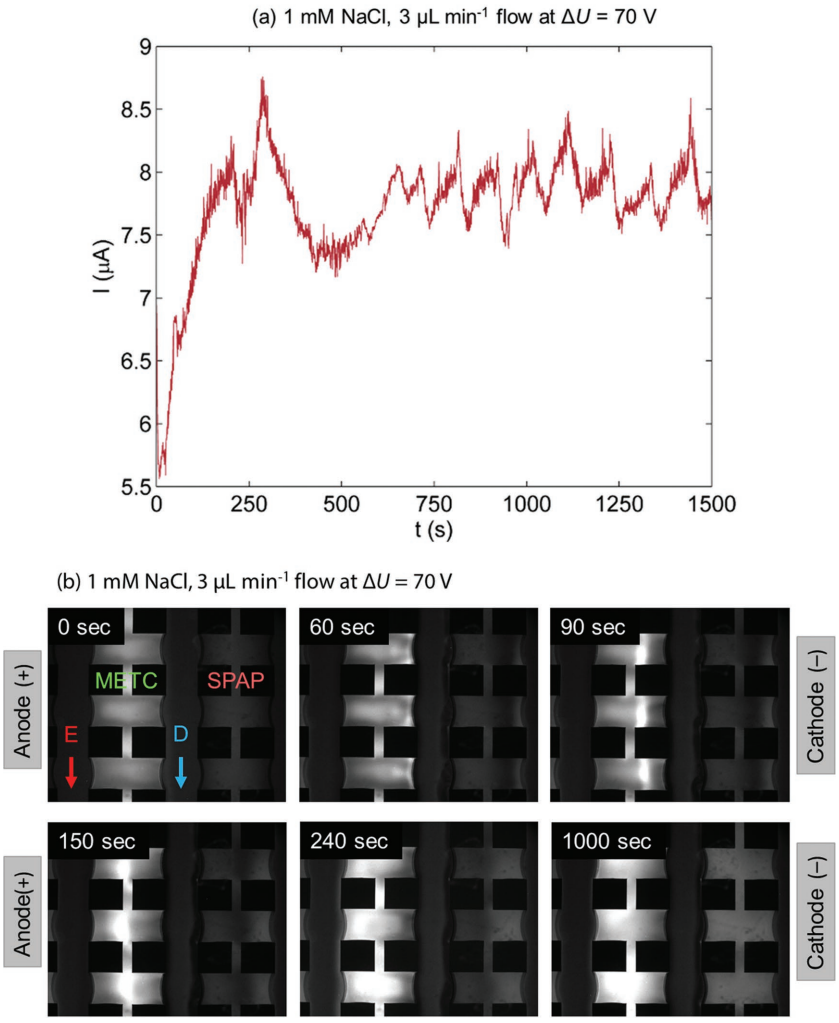

Figure 7. The design of the microfluidic electrodialysis platform allows visualization of transport in the hydrogels between the salt enriched (E) and depleted (D) channels. In panel (a), the current I is plotted as function of time t for a fixed potential difference of $\Delta U = 70$ V and flow rate of 3 μL min^{-1}. Before reaching steady state, the change in current can be related to transport in the hydrogel, as indicated by the b) fluorescence images of the dye in the hydrogels (1×10^{-3} M NaCl solution with 5×10^{-6} M Alexa Fluor 488 Cadaverine). It took about 600 s before the intensity, and thus presumably dye and ion concentration in the hydrogels, was constant.

balance between the degree of swelling and the charge density. The material properties were characterized, and the ion exchange hydrogels showed ion-selective permeation, based on their ion exchange capacity, permselectivity, and resistivity. We demonstrated that a device with patterned hydrogels can be used for desalination of water with salt concentrations up to 1×10^{-3} M NaCl at various flow rates (0–5 μL min^{-1}), applied potentials (0–100 V), and current densities (12–28 A m^{-2}). We obtained alternating dilute and concentrated streams at the outlet of the microchip. We achieved a desalination degree of 40% for an inlet concentration of 1×10^{-3} M NaCl, an applied potential difference of $\Delta U = 70$ V and a flow rate of 3 μL min^{-1}. The maximum desalination degree obtained was 75%.

By utilizing a charged fluorescent dye, we could visualize the ion concentration in the ED device. The fluorescence images revealed that ion-depleted boundary layers are formed near the ion-exchange hydrogels when a potential difference ΔU is applied. When $\Delta U > 25$ V, we observed the formation of vortices, enhancing convective transport toward the hydrogels in the overlimiting current regime. The desalination platform described here thus enables visualization of charge transport through the hydrogels, which can contribute to a better understanding of the transport phenomena in ED processes.

The separation efficiency can be enhanced by increasing the total length of the hydrogel–liquid interface by increasing the residence time of the solution in the microchannels, or by optimizing the hydrogel properties like the charge density. This would allow desalination of salt solutions with higher concentrations without the need to apply large potential differences. Our approach might, therefore, be promising for the development of processes related to water desalination,[39] sample pretreatment,[40] and high focusing of proteins.[41]

4. Experimental Section

Microchip and Hydrogel Fabrication: The SU-8 masters of the PDMS microchips were fabricated in the MESA+ cleanroom facility at the University of Twente. The masters consisted of two layers of SU-8. The widths of the microchannels and the pillars were 700 and 1720 μm, respectively. The first layer contained the pillar layout and its thickness was measured as 67.5 μm (Bruker Dektak, Germany). The second layer contained both pillar and capillary barrier layouts with a width of 2.0 μm and a thickness of 7.5 μm (see Figure 1b and Supporting information S3).

The microchip was fabricated by assembling a PDMS layer with a microscope slide. To achieve that, PDMS precursor was prepared, degassed, poured onto the master, and cured. The cured PDMS was peeled off from the master and treated with oxygen plasma to ensure irreversible bonding with the microscope slide. All microchannels, pillars, capillary barriers, inlets, and outlets were structured in the PDMS layer.

All hydrogel solutions (each with a volume of 500 μL) were degassed at 7 kPa vacuum for 15 min immediately prior to use. All hydrogel precursors were prepared in a nitrogen environment by blending 20% v/v of acrylamide/bis (19:1) (BioRad), 15% w/v *N,N′*-bis(2-hydroxyethyl) ethylenediamine (bis, Sigma-Aldrich), 10% w/v of DMPA (Invitrogen), and 5% w/v of ammonium persulfate (Invitrogen) solutions in a flow hood to avoid dust particles. For the AEHs, 1% v/v METC solution (Sigma-Aldrich), and for the CEHs, 1% w/v SPAP salt (Sigma-Aldrich) were added to the acrylamide/bis mixture. As the cross-linking reaction was inhibited by oxygen, patterning and polymerization processes were performed in a nitrogen environment.

Figure 2 shows the microchip fabrication and hydrogel patterning processes. A detailed explanation of the capillary pinning technique was reported by Gumuscu et al.[20] After the degassing process, ≈1 µL of AEH and CEH solutions was alternatingly pipetted into the parallel columns by capillary action. Hydrogel precursors remained contained between the PDMS pillars due to capillary pinning at the barriers. Patterned precursors were then exposed to UV light at 400 mW cm^{-2} for 3 min. Microchips containing CEH and AEH were immersed in 0.1×10^{-3} M NaCl solution at room temperature. The microchip had six microchannels, which were connected by alternating AEH and CEH as shown in Figure 1b.

Scanning Electron Microscopy (SEM): Thin films of polymerized hydrogels were cast on a glass surface and freeze-dried for 2 d. Samples were kept in a vacuum chamber overnight and subsequently coated with a 5 nm layer of chromium using a sputtering device (E5000 sputter coater, USA). SEM images were taken using an FEI Sirion HR-SEM.

FTIR and XPS: FTIR spectra were measured with a Bruker ALPHA (Bruker Optics, Germany) using an attenuated total reflectance attachment. Polymerized hydrogels were freeze-dried for 2 d in Eppendorf tubes and kept in a vacuum chamber overnight. Dried samples were directly analyzed without any further sample preparation. For XPS, 1 g of both polymerized AEH and CEH were freeze-dried for 2 d in Eppendorf tubes and kept in a vacuum chamber overnight. Dried samples were analyzed using a Quantera SXM (Physical Electronics).

Ion Exchange Capacity (IEC): The IEC was the amount of charged groups in the hydrogels and was measured by titration.[42] For the titration of AEH, 0.7 g of the hydrogel was immersed in 3 M NaCl (Sigma-Aldrich) for 3 d at room temperature to exchange all counterions in the AEH for Cl^-. After rinsing it with deionized water, the chloride ions were replaced by sulfate ions by immersing the hydrogel into a 1.5 M Na_2SO_4 solution for 3 h. The Na_2SO_4 solution was refreshed every hour of the experiment and the collected solutions were titrated with 0.1 M $AgNO_3$ solution. The required volume of $AgNO_3$ was recorded. The hydrogel was dried in a vacuum oven at 60 °C for 48 h and its dry weight was recorded for IEC calculations. For the titration of CEH, 0.7 g of the hydrogel was immersed in 1 M HCl solution for 3 d at room temperature to exchange all counterions in the CEH for H^+. The hydrogel was then rinsed with deionized water and immersed in a 2 M NaCl solution for 3 h to replace the hydrogen ions for sodium ions. The NaCl solution was refreshed every hour and the refreshed solutions were collected in a separate container. The collected solutions were then titrated with 0.1 M NaOH solution. The hydrogel was similarly dried and its weight was measured for IEC calculations. All of these experiments were repeated three times.

Water Swelling: Water swelling of the hydrogels was determined by immersion in deionized water and subsequent drying in a vacuum oven. The degree of water swelling WS was calculated using the following equation: $WS = (W_s - W_d)/W_d$. Here, W_s and W_d represent the weight of the swollen hydrogels and the dried hydrogels, respectively. Also the swelling degree of the polymerized hydrogels was tested by immersing 2 mL of bulk hydrogel after polymerization in 50 mL deionized water, and by immersing the patterned hydrogels on the chip in DI water for 72 and 16 h, respectively.

Permselectivity: Permselectivity determines the capability of the hydrogel to discriminate between anions and cations. An in-house-built two-compartment cell made of plexiglass was used in permselectivity experiments. The charged hydrogel was located in between two compartments. One of the compartments was filled with 0.1 M NaCl solution while the other compartment was filled with 0.5 M NaCl solution using a peristaltic pump. Both solutions were recirculated continuously during the measurement and kept at 25 °C using a thermostatic bath. Two reference calomel electrodes were used to measure the electric potential over the hydrogel by connecting the system to a potentiostat (Metrohm Autolab PGSTAT302N, the Netherlands) for monitoring the changes in voltage over the hydrogel. The apparent permselectivity $\alpha = \Delta U_{meas}/\Delta U_{theor}$ was calculated for both AEH and CEH separately using the ratio of the measured potential difference ΔU_{meas} over the theoretical potential difference ΔU_{theor} for an ideal permselective membrane. The theoretical potential difference was obtained from the Nernst equation $\Delta U_{theor} = (RT)/(zF)\ \ln(c_1\gamma_1/c_2\gamma_2)$. Here, R is the gas constant, T is the temperature, z is the electrochemical valence, and F is the Faraday constant.[43] The salt concentrations and activity coefficients of the two solutions are indicated by c_i and γ_i, where γ_i denotes the mean activity coefficient for NaCl solutions in water at 25 °C as obtained from Sata et al.[44]

Membrane Resistivity: The area resistance of both AEH and CEH was measured using an in-house-built six-compartment cell made of plexiglass. In experiments, 0.1 M NaCl was used and the voltage drop ΔU over the hydrogel was recorded for an applied current density I/A. Here, I is the current through the membrane with area A. The resistivity $R\rho$ of each hydrogel, after baseline correction by performing a blank run, was given by the slope of the potential difference versus current density curve. Thus, $R\rho = (A\Delta U)/(Id)$, d being the thickness of the hydrogel.

Electrodialysis Experiments: The desalination performance of the microchip was investigated using solutions of different NaCl concentrations (0.01×10^{-3}, 0.1×10^{-3}, and 1×10^{-3} M) containing 5×10^{-6} M of Alexa Fluor 488 Cadaverine (ThermoFisher Scientific), a negatively charged fluorescent dye. This dye is utilized to qualitatively determine the local ion concentration in the microchannels. Gold-coated copper electrodes were placed in the outer two microchannels adjacent to the hydrogels. An electrical potential or current was applied by a Keithley 2450 Source Meter, controlled by a home-built LabVIEW program. The fluorescent dye was visualized using a Hamamatsu ORCA-Flash4.0 LT camera mounted on an inverted Zeiss Axiovert 40 MAT microscope. The liquid flow was supplied to the microchip using Harvard Picoplus programmable syringe pumps and Braun Omnifix-F 1 mL syringes. The samples were collected separately from each microchannel and the conductivity of the samples was measured using a potentiostat (BioLogic SP300, France) combined with an in-house-made interdigitated electrode sensor. A calibration curve was plotted and used for the salt concentration conversions (Supporting information S6).

Supporting Information

Supporting Information is available from the Wiley Online Library or from the author.

Acknowledgements

B.G., A.S.H., and A.M.B. contributed equally to this work. This work was funded by the Dutch network for Nanotechnology NanoNext NL, in the subprogram "Nanofluidics for Lab-on-a-chip". R.G.H.L. acknowledges support from the European Research Council for the ERC starting grant 307342-TRAM. The authors also thank Mark Smithers for SEM imaging, Mark Ankoné for freeze-drying, Timon Rijnaarts for permselectivity and resistivity measurements, and Jan van Nieuwkasteele for technical support. Abstract and introduction of this manuscript were corrected on December 20, 2016, following initial online publication.

Received: June 28, 2016
Revised: September 5, 2016
Published online: October 28, 2016

[1] H. Strathmann, *Desalination* **2010**, *264*, 268.
[2] M. Tedesco, H. V. M. Hamelers, P. M. Biesheuvel, *J. Membr. Sci.* **2016**, *510*, 370.
[3] V. V. Nikonenko, N. D. Pismenskaya, E. I. Belova, P. Sistat, P. Huguet, G. Pourcelly, C. Larchet, *Adv. Colloid Interface Sci.* **2010**, *160*, 101.

[4] R. W. Baker, *Pervaporation–Membrane Technology and Applications*, Wiley, Chichester **2004**.
[5] I. Rubinstein, B. Zaltzman, *J. Fluid Mech.* **2013**, *728*, 239.
[6] M. B. Andersen, M. Van Soestbergen, A. Mani, H. Bruus, P. M. Biesheuvel, M. Z. Bazant, *Phys. Rev. Let.* **2012**, *109*, 108301.
[7] F. Maletzki, H. W. Rösler, E. Staude, *J. Membr. Sci.* **1992**, *71*, 105.
[8] V. V. Nikonenko, A. V. Kovalenko, M. K. Urtenov, N. D. Pismenskaya, J. Han, P. Sistat, G. Pourcelly, *Desalination* **2014**, *342*, 85.
[9] E. D. Belashova, N. A. Melnik, N. D. Pismenskaya, K. A. Shevtsova, A. V. Nebavsky, K. A. Lebedev, V. V. Nikonenko, *Electrochim. Acta* **2012**, *59*, 412.
[10] T. A. Zangle, A. Mani, J. G. Santiago, *Chem. Soc. Rev.* **2010**, *39*, 1014.
[11] J. H. Lee, Y. A. Song, J. Han, *Lab Chip* **2008**, *8*, 596.
[12] S. J. Kim, S. H. Ko, R. Kwak, J. D. Posner, K. H. Kang, J. Han, *Nanoscale* **2012**, *4*, 7406.
[13] R. Kwak, G. Guan, W. K. Peng, J. Han, *Desalination* **2013**, *308*, 138.
[14] L. J. Cheng, H. C. Chang, *Biomicrofluidics* **2011**, *5*, 046502.
[15] S. J. Kim, S. H. Ko, K. H. Kang, J. Han, *Nat. Nanotechnol.* **2010**, *5*, 297.
[16] M. Kim, M. Jia, T. Kim, *Analyst* **2013**, *138*, 1370.
[17] S. Park, T. D. Chung, H. C. Kim, *Microfluid. Nanofluid.* **2009**, *6*, 315.
[18] Y. Zhang, N. E. Benes, R. G. H. Lammertink, *Lab Chip* **2015**, *15*, 575.
[19] D. Hlushkou, R. Dhopeshwarkar, R. M. Crooks, U. Tallarek, *Lab Chip* **2008**, *8*, 1153.
[20] B. Gumuscu, J. G. Bomer, A. van den Berg, J. C. T. Eijkel, *Lab Chip* **2015**, *15*, 664.
[21] B. Gumuscu, J. G. Bomer, A. van den Berg, J. C. T. Eijkel, *Biomacromolecules* **2015**, *16*, 3802.
[22] W. Zhao, P. Fonsny, P. FitzGerald, G. G. Warr, S. Perrier, *Polym. Chem.* **2013**, *4*, 2140.
[23] M. Balastre, S. J. Kostka, M. McMillan, *U.S. Patent Application No. 14/527,812*, **2014**.
[24] S. Scognamillo, V. Alzari, D. Nuvoli, J. Illescas, S. Marceddu, A. Mariani, *J. Polym. Sci., Part A: Polym. Chem.* **2011**, *49*, 1228.
[25] V. V. Khutoryanskiy, Z. S. Nurkeeva, G. A. Mun, A. D. Sergaziyev, Z. Ryskalieva, J. M. Rosiak, *Eur. Polym. J.* **2003**, *39*, 761.
[26] P. M. Biesheuvel, A. P. Van Loon, R. Raangs, H. Verweij, C. Dirksen, *Eur. J. Soil Sci.* **2000**, *51*, 355.
[27] O. Okay, in *Hydrogel Sensors and Actuators* (Eds: G. Gerlach, K.-F. Arndt), Springer,Berlin **2009**, p. 1.
[28] S. Durmaz, O. Okay, *Polymer* **2000**, *41*, 3693.
[29] E. Pretsch, P. Bühlmann, C. Affolter, E. Pretsch, P. Bhuhlmann, C. Affolter, *Structure Determination of Organic Compounds*, Vol. 13, Springer, Berlin **2009**.
[30] Y. L. Ji, Q. F. An, Q. Zhao, W. D. Sun, K. R. Lee, H. L. Chen, C. J. Gao, *J. Membr. Sci.* **2012**, *390*, 243.
[31] G. Beamson, D. Briggs, *High Resolution XPS of Organic Polymers: The Scienta ESCA300 Database*, John Wiley & Sons, Chichester **1992**.
[32] P. Cardiano, P. G. Mineo, F. Neri, S. L. Schiavo, P. Piraino, *J. Mater. Chem.* **2008**, *18*, 1253.
[33] P. Długołęcki, K. Nymeijer, S. Metz, M. Wessling, *J. Membr. Sci.* **2008**, *319*, 214.
[34] T. Xu, *J. Membr. Sci.* **2005**, *263*, 1.
[35] A. H. Galama, J. W. Post, M. C. Stuart, P. M. Biesheuvel, *J. Memb. Sci.* **2013**, *442*, 131.
[36] T. Sata, *Ion Exchange Membranes*, Royal Society of Chemistry, Cambridge **2004**.
[37] N. Panchuk-Voloshina, R. P. Haugland, J. Bishop-Stewart, M. K. Bhalgat, P. J. Millard, F. Mao, W. Y. Leung, R. P. Haugland, *J. Histochem. Cytochem.* **1999**, *47*, 1179.
[38] S. M. Davidson, M. Wessling, A. Mani, *Sci. Rep.* **2016**, *6*, 22505.
[39] K. N. Knust, D. Hlushkou, R. K. Anand, U. Tallarek, R. M. Crooks, *Angew. Chem., Int. Ed.* **2013**, *52*, 8107.
[40] P. Kubáň, A. Šlampová, P. Boček, *Electrophoresis* **2010**, *31*, 768.
[41] R. S. Foote, J. Khandurina, S. C. Jacobson, J. M. Ramsey, *Anal. Chem.* **2005**, *77*, 57.
[42] H. Strathmann, *Membr. Sci. Technol. Ser.* **2004**, *9*, 89.
[43] R. C. Weast, D. R. Lide, M. J. K. Astle, W. H. Beyer, *Handbook of Chemistry and Physics*, 76th ed. (Ed: D. R. Lide), CRC Press, Boca Raton, FL **1989**.
[44] T. Sata, *Ion Exchange Membranes: Preparation, Characterization, Modification and Application*, Royal Society of Chemistry, Cambridge, **2004**.